Vibrational Spectroscopy 72 (2014) 20–25

Contents lists available at ScienceDirect

Vibrational Spectroscopy

journal homepage: www.elsevier.com/locate/vibspec

Infrared absorption spectrum of $HoFe_3(BO_3)_4$ crystal

S.N. Sofronova [a,b], Yu. V. Gerasimova [a,b,*], A.N. Vtyurin [a,b], I.A. Gudim [a,b], N.P. Shestakov [a,b], A.A. Ivanenko [a,b]

[a] Kirensky Institute of Physics SB RAS, Krasnoyarsk 660036, Russia
[b] Siberian Federal University, Krasnoyarsk 660079, Russia

ARTICLE INFO

Article history:
Received 11 July 2013
Received in revised form 4 February 2014
Accepted 5 February 2014
Available online 21 February 2014

Keywords:
Holmium ferroborate
Infrared absorption

ABSTRACT

Infrared (IR) absorption spectra of $HoFe_3(BO_3)_4$ crystal have been obtained in spectral range 30–7000 cm^{-1} at temperatures from 4 to 423 K. Vibrational frequencies have been simulated with 'Lady' software package both for high-temperature and low-temperature phases. The experimental spectra have been analyzed on the basis of calculated data, and interpreted within the framework of internal vibrations of ionic complexes of $HoFe_3(BO_3)_4$ crystal lattice. The spectral range under study was observed to have no Davydov splitting of internal vibrational modes due to unit cell multiplication. No effects of magnetic ordering on the IR spectra of the crystal under study were observed in the low-temperature range.

1. Introduction

Crystal of rare-earth ferroborate $HoFe_3(BO_3)_4$ belongs to the family of oxyborates with general formula $ReM_3(BO_3)_4$ (where *Re* is the rare-earth ion, *M* = Fe, Al, Ga, Cr) [1–3]. Researchers' interest to these compounds is generated primarily by applications of isomorphic alumoborates in optic and optoelectronic devices [4,5], and by specific magnetic properties of ferroborates, e.g. great magnetoelectric effect [6–8]. These properties are assumed to be due to two interacting magnetic subsystems associated with ions of iron and rare-earth ions, respectively. In addition, recently several ferroborates were found to possess spontaneous polarization; consequently, these compounds may be considered as multiferroics featuring both ferromagnetic and ferroelectric properties [9]; this makes $ReFe_3(BO_3)_4$ crystals attractive not only to develop fundamental notions, but also to develop promising applications, e.g. in spintronic devices. To interpret mechanisms and value of magnetoelectric relations it is necessary to know the structure of crystal vibrational spectrum and mechanisms of its formation.

2. Crystal structure

At high temperatures the rare-earth ferroborates exhibit the structure of huntite crystals that belong to space group $R32$ (D_3^7) with three formula units per unit cell (Fig. 1). Under cooling several ferroborates (with rare-earth ions of small ionic radius) undergo structural phase transition with symmetry reducing to $P3_121$ (D_3^4). The temperature of this transition depends on the ionic radius of the rare-earth ion (the smaller the radius the higher the temperature) and for $HoFe_3(BO_3)_4$ crystal it ranges from 360 to 430 K depending on the conditions of crystal growth [11,12]. For our samples grown by flux-melt technique [12] the structural phase transition was observed at 360 K.

Main structural elements of rare-earth ferroborates are FeO_6 octahedra, BO_3 triangles and triangular prisms ReO_6. The octahedra are connected by edges forming helical chains along *c* axis (Fig. 1). The chains of octahedra are connected by prisms ReO_6 and triangles BO_3. In the high-temperature phase all three chains running through the unit cell are equivalent. Local symmetry of the rare-earth ion (triangular prisms ReO_6) is D_3. Local symmetry of boron ions is different: the symmetry of boron ion in 3b position (B^1), whose oxygen environment forms an equilateral triangle and are connected with the chains of FeO_6, is D_3 (Fig. 1). The symmetry of boron ions in 9e position (B^2) is C_2, isosceles triangles BO_3 are connected in this case with two triangular prisms ReO_6 and chains of octahedra FeO_6.

Structural phase transition shifts one of the chains of FeO_6 octahedra along the *c*-axis relative to two others (the shift is ~0.066 Å) [13]. Some of the triangular B^2O_3 groups (connecting triangular ReO_6 prisms and chains of FeO_6 octahedra) become distorted and turn around their axis by approximately 7°, and their local symmetry is reduced to C_1. The symmetry of triangular B^1O_3 groups connecting chains of FeO_6 octahedra is reduced from D_3 to

* Corresponding author at: Kirensky Institute of Physics SB RAS, Krasnoyarsk 660036, Russia. Tel.: +7 923 273 1745; fax: +7 391 243 89 23.
E-mail address: jul@iph.krasn.ru (Yu.V. Gerasimova).

http://dx.doi.org/10.1016/j.vibspec.2014.02.005
0924-2031/

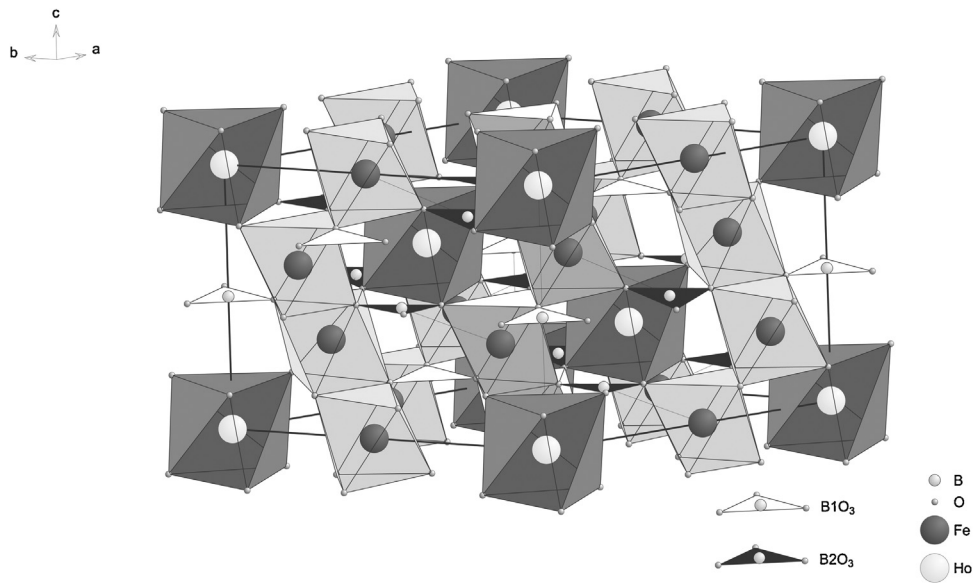

Fig. 1. Huntite structure. Crystal unit cell in a hexagonal system; FeO_6 octahedrons, ReO_6 prisms and BO_3 triangles are shown. Chains of FeO_6 octahedrons are equivalent in the high temperature phase; different colors correspond to the low temperature phase structure.

C_2 due to the distortion and shift of the boron ion by approximately 0.12 Å. The local symmetry of the rare-earth ion is also reduced from D_3 to C_2.

The above described changes of local symmetry of the structural units and tripling of the unit cell volume should bring forth new modes in the vibrational spectrum.

The factor group analysis performed by Fausti et al. [14] predicts 60 normal vibrational modes existing in the high temperature $R32$ phase:

$$\Gamma = 7A_1(xx, yy, zz) + 13A_2(E \parallel z) + 20E(E \parallel x\ , E \parallel y\ , xz, yz, xy),$$

optical vibrations among them are: $7A_1$, $12A_2$, $19E$. The notations given in parentheses refer to the allowed components of electric dipole moment (IR activity) and polarizability tensor (Raman activity).

In the low temperature $P3_121$ phase comprising three formula units per the unit cell, 180 normal vibrational modes are predicted, accordingly:

$$\Gamma = 27A_1 + 33A_2 + 60E,$$

optical vibrations among them are: $27A_1$, $32A_2$, $59E$. Here A_2 and twice degenerate E modes are active in IR absorption spectra; transverse (TO) E modes propagate along the c-axis ($k \parallel c$), while LO E mode go perpendicular to c-axis. The results of symmetry analysis for the vibrational modes of high and low temperature phases and the correlation diagram are given in ref. [14].

Raman scattering investigations of $HoFe_3(BO_3)_4$ below the transition temperature [12] have shown soft mode restoration connected supposedly with this structure transformation. Restoring mode was found in xx, yy, zz Raman components and attributed to A_1 representation; therefore it should be inactive in IR absorption spectra. Possible mechanism of this structural transition was discussed in [15], where it was attributed to the instability of transversal acoustic mode at $k = (b_1 + b_2 + b_3)/3$. This assumption cannot be verified by IR spectroscopy where phonons of the center of Brillouin zone only are active. Therefore below the structural phase transition we can expect only appearance of some new lines in IR spectra due to unit cell multiplication.

Beside the structural phase transition, an ordered antiferromagnetic state has been found in this crystal below 38 K. The major feature of the spin ordering observed in Raman spectra was the arising of a broad structured scattering band around 60 cm^{-1} ascribed to two-magnon Raman scattering involving the creation of magnon pairs. Below T_N this is a characteristic feature for all investigated compounds of the $ReFe_3(BO_3)_4$ family[14], but this "magnon" mode as well can be observed in Raman spectra only.

Another interesting feature is the dielectric anomalies below the Neel temperature transition observed in $HoFe_3(BO_3)_4$ [16]. The similar behavior of the dielectric constant has been observed in $TbFe_3(BO_3)_4$; both materials exhibit an increase of ε_{ab} below T_N, which is truncated by spin-reorientation transition ($T_{sr} = 5$ K) in $HoFe_3(BO_3)_4$. Adem et al. [17] observed the shift of the transverse phonon frequency 200 cm^{-1} at T_N in $TbFe_3(BO_3)_4$. This anomalous softening of the TO phonon mode is a possible reason for the behavior of the dielectric constant. This behavior of dielectric constant looks very much alike in both compounds, so analogous dependence is quite probable in $HoFe_3(BO_3)_4$, too.

3. Experimental results and calculations

IR spectra were experimentally studied with a VERTEX 80V (Bruker) Fourier-transform spectrometer in the spectral range from 30 to 7500 cm^{-1} with spectral resolution 0.2 cm^{-1}. Temperature studies were conducted with an Optistat^{TM} AC-V 12a 0.25W4K cryostat in the temperature range from 4 to 423 K.

The spectra in the mid-IR range (370–7500 cm^{-1}) were studied in KBr pellet samples, 13 mm in diameter and ≈0.55 mm thick. To prepare the pellets, the compound under study was thoroughly ground in a mortar with 0.2 g of KBr at 1:100 ratio. The mixture produced was vacuum-pressed with hydraulic press at a pressure of 10×10^4 N/cm^2. To produce the mid-IR range spectra, a Globar (U arc of silicon carbide) was used as a light source, with RT-DLaTGS sensor and Ge/KBr beamsplitter.

The spectra in the far IR (30–100 cm^{-1}) and far-middle IR (85–680 cm^{-1}) ranges were studied on compressed pellet samples 13 mm in diameter and ≈0.8 mm thick. The tablets were prepared as follows: the compound under study was thoroughly ground in a mortar with 0.1 g of fine polyethylene at 1:100 ratio. The mixture was pressed in a mold at 423 K temperature by hydraulic press at a pressure of 2×10^4 N/cm^2. To produce the spectra in the 30–100 cm^{-1} spectral range, an ultra-high pressure mercury lamp was used as light source, with a RT-DTGS FIR detector, and a

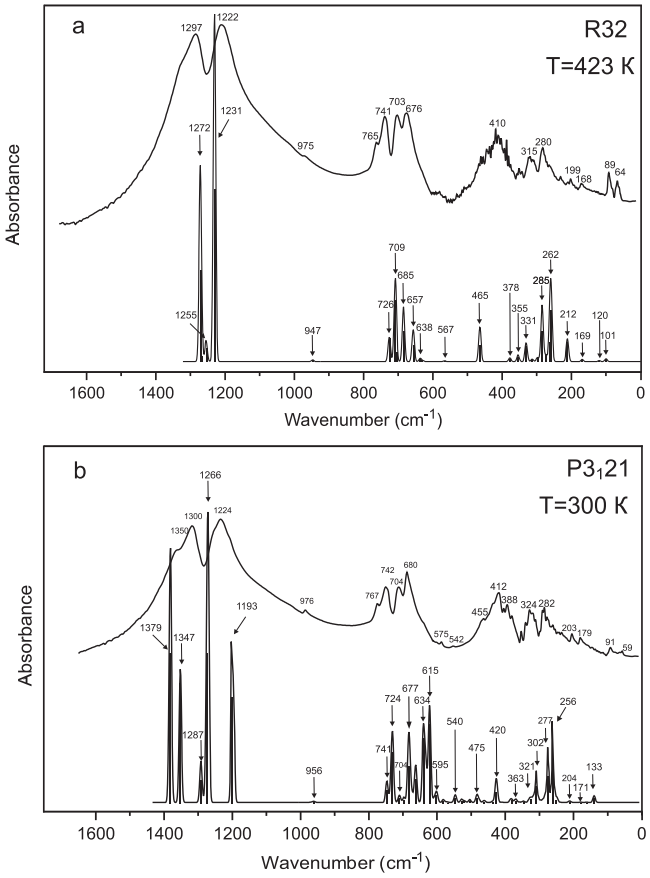

Fig. 2. Experimental and simulated IR spectra of $HoFe_3(BO_3)_4$ crystal in the high temperature phase *R*32 (a) and low temperature phase $P3_121$ (b).

Mylar Multilayer beamsplitter. In the 85–680 cm^{-1} spectral range, we used a Globar (U arc of silicon carbide) for light source, a Mylar Multilayer beamsplitter, and a RT-DTGS FIR detector.

The IR spectra were analyzed with OriginPro 8 software package. For several frequency ranges complex bands were deconvoluted into individual Lorentzian contours.

The IR spectra obtained for these spectral ranges and their temperature transformations are shown in Figs. 2–7.

To interpret the results, the vibrational spectrum was simulated empirically using the 'Lady' software package [18] both in the high temperature and low temperature phases. The calculated vibrational spectra in the high and low temperature phases are in good agreement with the experimental ones (Fig. 2); the frequencies of the simulated IR active lines are also given in Table 1. Tables 2 and 3 present the eigenvectors of simulated modes for high and low temperature phases, respectively. It should be pointed out that the empirical model of lattice dynamics used does not take into account splitting of degenerate polar *E* modes into LO and TO components.

4. Discussion

Let's consider selected spectral ranges in more detail. Temperature studies in the high temperature phase (360–423 K) were carried out both in the medium and the far IR spectra; however considerable noise in the absorption spectra (see Fig. 2a) in the lower frequency range (30–600 cm^{-1}) impedes deconvolution of complex bands into individual lines here to perform quantitative analysis of their parameters. Fig. 3 shows evolution of the absorption spectra in the range 500–1700 cm^{-1} near the structural phase

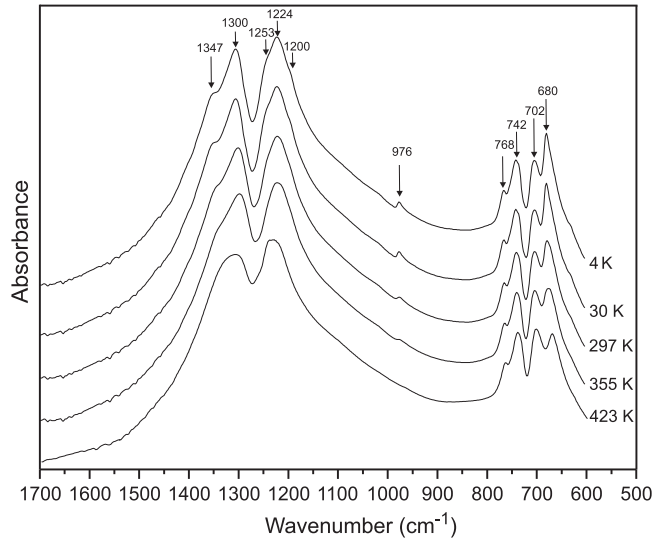

Fig. 3. Temperature transformation of absorption spectra in frequency range 1700–500 cm^{-1}.

transition. From the figure it is obvious that spectra do not undergo any considerable changes under cooling.

As mentioned earlier, the main structural elements of rare-earth ferroborates are octahedra FeO_6, triangles BO_3 and triangular prisms ReO_6. Internal frequencies of free planar group BO_3 are: $\nu_1(A_1) = 1060\,cm^{-1}$, $\nu_2(A_2) = 648–668\,cm^{-1}$, $\nu_3(E) = 1428–1490\,cm^{-1}$, $\nu_4(E) = 545–606\,cm^{-1}$ [19].

At 423 K the spectrum was found to have two broad bands with maxima at 1224 cm^{-1} and 1300 cm^{-1}. The broad asymmetrical band at 1300 cm^{-1} is determined by the stretching vibration ν_3 of BO_3 group with symmetry C_{2v}. Low site symmetry of BO_3 group results in the line splitting. Under cooling below the transition point site symmetry of BO_3 group is reduced to C_1, this splitting increases and spectral line 1300 cm^{-1} exhibits a distinct shoulder with maximum at 1347 cm^{-1}.

The broad band with two maxima at about 1224 cm^{-1} is determined by stretching vibrations ν_3 of BO_3 group with symmetry D_3, the doublet structure of this line seems to be induced by the Fermi resonance of vibrations ν_3 and overtone ν_4 of BO_3 group, which were earlier observed in IR spectra of relative compounds [14]. As the temperature decreases, lines split because of symmetry reduction of BO_3 to C_2, as a result the spectral line can be observed to have two arms with maxima at 1200 cm^{-1} and 1253 cm^{-1}.

In the range 900–1000 cm^{-1} a new low-intensity line at 976 cm^{-1} emerges in the spectrum below the phase transition. New emerging lines corresponding to *E* modes after the phase transition were observed earlier in this range of the Raman spectrum of $GdFe_3(BO_3)_4$ [14]. We attribute spectral lines in the frequency range 650–780 cm^{-1} to bending vibrations ν_4 of BO_3 groups.

Fig. 4 shows IR spectra in the range from 100 to 600 cm^{-1} in the low temperature phase. As seen in Fig. 4, the range from 180 to 500 cm^{-1} exhibits a fairly complex contour comprising a great number of maxima. This frequency range corresponds to internal vibrations of FeO_6 and triangular prisms ReO_6, and external lattice vibrations. As the symmetry of FeO_6 octahedra and triangular prisms ReO_6 in the low-temperature phase is quite low (C_2), many internal vibrations of these groups split. The authors of [10], who studied IR spectra of $TbFe_3(BO_3)_4$ crystal, interpreted spectral lines at 280 cm^{-1} and 440 cm^{-1} as bending and stretching modes of $(FeO_6)^{9-}$ octahedron, respectively. In our IR spectrum we also observe fairly intensive lines at about 280 cm^{-1} and 410 cm^{-1}; taking into consideration that parameters of $(FeO_6)^{9-}$ octahedra in our compound and in $TbFe_3(BO_3)_4$ are similar we think that these

Table 1
Calculated vibrational frequencies of $HoFe_3(BO_3)_4$ crystal in the height – ($R32$ (D_3^7)) and the low – ($P3_121$ (D_3^4)) temperature phases.

$R32$ (D_3^7)			$P3_121$ (D_3^4)					
A_1 Raman active	A_2 IR active	E doubly degenerate, IR and Raman active	A_1 Raman active	A_2 IR active		E doubly degenerate, IR and Raman active		
178.1	100.6	120.4	139.2	132.7	540.2	141.7	320.9	627.1
327.5	169.3	170.3	163.1	149.0	599.7	154.7	333.7	633.6
486.6	212.1	214.6	183.3	162.7	615.3	171.2	340.0	656.0
645.7	233.7	229.3	208.8	183.1	626.5	180.5	344.1	673.1
941.7	258.9	261.8	234.8	204.3	665.4	197.8	362.6	690.7
973.5	273.7	285.1	279.7	249.0	676.7	204.4	404.0	704.1
1233.8	298.3	313.5	295.9	256.2	677.6	207.8	419.7	724.2
	331.3	354.6	321.0	277.0	727.9	224.6	430.2	740.7
	630.1	378.3	332.8	278.0	955.7	230.2	455.4	948.9
	709.0	464.8	357.0	290.4	1194.2	241.9	469.5	951.8
	726.4	566.7	391.3	295.0	1269.0	255.2	476.8	963.4
	1270.6	637.6	450.8	302.5	1347.0	268.5	498.6	995.0
		657.3	482.4	314.2	1378.8	272.1	513.1	1193.4
		685.4	513.3	350.9		275.1	521.7	1195.2
		708.1	528.5	372.7		293.2	538.7	1265.6
		947.4	633.4	377.4		300.4	564.5	1269.3
		1231.0	638.9	454.0		305.3	575.0	1286.6
		1255.3	646.8	474.6		307.7	594.5	1347.1
		1271.9	705.0	497.5		312.9	604.6	1376.3
			731.4				616.5	1378.8
			946.6					
			965.6					
			989.2					
			1195.8					
			1266.8					
			1286.2					
			1376.5					

lines are bending and stretching vibrations of $(FeO_6)^{9-}$ octahedrons as well. The lowest-frequency vibrations (Fig. 5) are associated with external lattice vibrations and vibrations of triangular prisms ReO_6.

Only minor transformations, like line splitting or new line appearance, were found in IR spectra below structural phase transition, as seen in Figs. 2–4. Some spectral ranges with new weak lines appearance or slight splitting of broad bands below the structural phase transition are shown in Figs. 5–7. To distinguish changes induced by magnetic ordering spectra obtained below 38 K are shown by bold lines.

Fig. 5 demonstrates appearance of two new lines, 66 and 77 cm^{-1}, that we attribute to external vibrations together with the line at 59 cm^{-1}. No anomalies induced by magnetic ordering were observed in this low frequency range. Within our precision, frequencies of all these lines do not change under cooling, which correlates with minor distortions of lattice parameters: according to Ritter et al. [13], cooling from 520 K down to 2 K decreases parameter a from 7.57 to 7.54 Å and parameter c from 9.53 to 9.51 Å, which is less than 1%.

Interesting anomaly was found earlier in Raman spectra of $TbFe_3(BO_3)_4$ crystal below magnetic phase transition: frequency

Table 2
Eigenvectors of lattice modes for the high temperature phase ($R32$).

Wyckoff sites and coordinates of atoms (hexagonal cell)	Eigenvector components; two eigenvectors are given for doubly degenerate E modes (hexagonal cell)			
	A_1	A_2	E_1	E_2
$Re(3a)$, (0, 0, 0) $B^1(3b)$ (0, 0, 1/2)	(0, 0, 0)	(0, 0, c)	(a, a, 0)	(b, b, 0)
	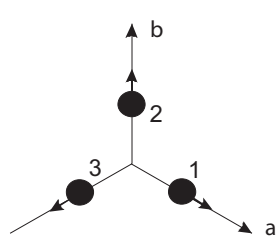	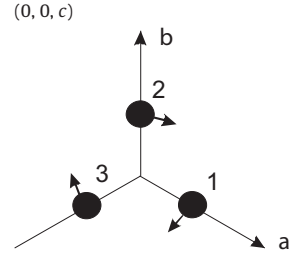		
Fe($9d$), O($9e$), $B^2(9e)$				
1(x, 0, z)			(a, b, c)	(m, n, k)
2(0, x, z)			(b, a,$-c$)	($-n$, $-m$, k)
3($-x$, $-x$, z)			(d, d, 0)	(l, $-l$, v)
O($18f$)				
(x, y, z)	($-a-b$,$-a$, c)	($-a-b$, $-a$, c)	(a, b, c)	(i, j, o)
($-y$, $x-y$, $z+1/3$)	(a, $-b$, c)	(a, $-b$, c)	(g, f, h)	(u, w, q)
($y-x$, $-x$, $z+2/3$)	(b, $a+b$, c)	(b, $a+b$, c)	(k, l, m)	(s, p, t)
(y, x, $-z$)	($-a$, $-a-b$, $-c$)	(a, $a+b$, c)	(b, a, $-c$)	($-j$, $-i$, o)
($x-y$, $-y$, $-z+2/3$)	($-b$, a, $-c$)	(b, $-a$, c)	(f, g, $-h$)	($-w$, $-u$, q)
($-x$, $y-x$, $-z+1/3$)	($a+b$, b, $-c$)	($-a-b$, $-b$, c)	(l, k, $-m$)	($-p$, $-s$, t)

Table 3
Eigenvectors of lattice modes for the low temperature phase ($P3_121$).

Wyckoff sites and coordinates of atoms (hexagonal cell)	Eigenvector components; two eigenvectors are given for doubly degenerate E modes (hexagonal cell)			
	A_1	A_2	E_1	E_2
	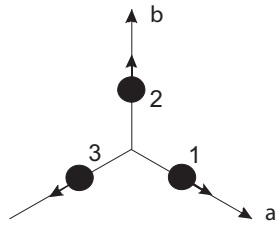	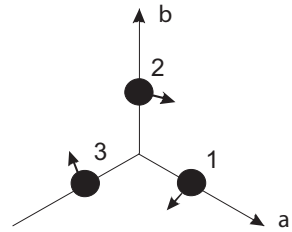		
Re(3*a*), B(3*b*), Fe(3*a*), O(3*b*)				
1(*x*, 0, *z*)			(*a*, *b*, *c*)	(*m*, *n*, *k*)
2(0, *x*, *z*+1/3)			(*b*, *a*, −*c*)	(−*n*, −*m*, *k*)
3(−*x*, −*x*, *z*+2/3)			(*d*, *d*, 0)	(*l*, −*l*, *v*)
Fe(6*c*), B(6*c*), O(6*c*)				
(*x*, *y*, *z*)	(−*a*−*b*, −*a*, *c*)	(−*a*−*b*, −*a*, *c*)	(*a*, *b*, *c*)	(*i*, *j*, *o*)
(−*y*, *x*−*y*, *z*+1/3)	(*a*, −*b*, *c*)	(*a*, −*b*, *c*)	(*g*, *f*, *h*)	(*u*, *w*, *q*)
(*y*−*x*, −*x*, *z*+2/3)	(*b*, *a*+*b*, *c*)	(*b*, *a*+*b*, *c*)	(*k*, *l*, *m*)	(*s*, *p*, *t*)
(*y*, *x*, −*z*)	(−*a*, −*a*−*b*, −*c*)	(*a*, *a*+*b*, *c*)	(*b*, *a*, −*c*)	(−*j*, −*i*, *o*)
(*x*−*y*, −*y*, −*z*+2/3)	(−*b*, *a*,−*c*)	(*b*, −*a*, *c*)	(*f*, *g*, −*h*)	(−*w*, −*u*, *q*)
(−*x*, *y*−*x*, −*z*+1/3)	(*a*+*b*, *b*, −*c*)	(−*a*−*b*, −*b*, *c*)	(*l*, *k*, −*m*)	(−*p*, −*s*, *t*)

of TO phonon near 200 cm^{-1} increased by several cm^{-1} while corresponding LO phonon remained constant at 205 cm^{-1}. The same spectral range for $HoFe_3(BO_3)_4$ is shown in Fig. 6: here two spectral lines at 205 and 200 cm^{-1} merge under cooling into one broader band with maximum at 203 cm^{-1}. At the same time the broad maximum at 173 cm^{-1} splits in two at 173 and 180 cm^{-1}. The intensities of these lines are quite small, so it is impossible to identify if these changes are continuous or go step-wise at Neel temperature.

Fig. 7 demonstrates the appearance of a new line at 398 cm^{-1} below the structural phase transition as well as splitting of the peaks at 410 and 460 cm^{-1}; no distinct anomalies were found near the magnetic transition in this range as well.

Comparison of Table 1 and Figs. 2 and 3 show that the tripling of the unit cell after the structural phase transition results in emergence of many new lines associated with Brillouin zone reduction (Davydov splitting), however, this splitting is quite small: e.g. in range 950 cm^{-1}, where below the transition the experimental spectrum has a low intensity line at 976 cm^{-1}, in the simulated spectrum before the transition there was one mode with frequency 947 cm^{-1}, and after the transition there are three modes with frequencies 949, 952, and 963 cm^{-1}. Only slight splitting of 410 cm^{-1} have been found in experimental spectra, that we interpreted as bending and stretching modes of $(FeO_6)^{9-}$ octahedrons; while our simulation predicts splitting of the corresponding mode at 464 cm^{-1} into three at 455, 469 and 476 cm^{-1} below the transition point.

In general experimental spectra below the structural phase transition exhibit less lines as compared to symmetry consideration; we attribute it to the fact that internal vibrations of complexes $(FeO_6)^{9-}$, $(BO_3)^{3-}$ and $(ReO_6)^{9-}$ are well localized and corresponding splittings are too small to be observed.

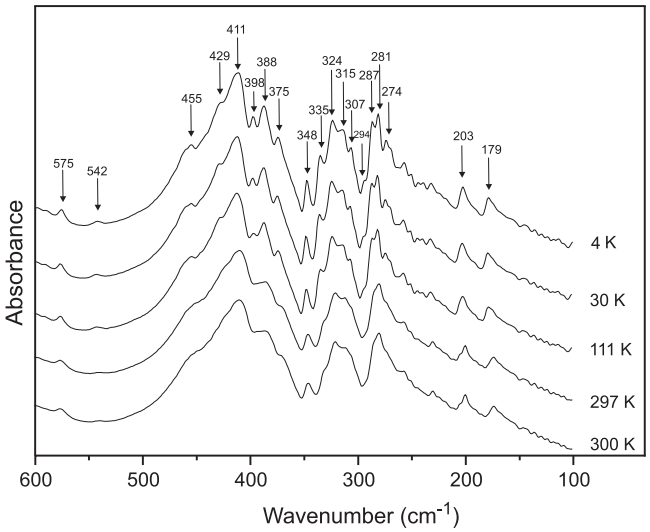

Fig. 4. Temperature transformation of absorption spectra in frequency range 600–100 cm^{-1}.

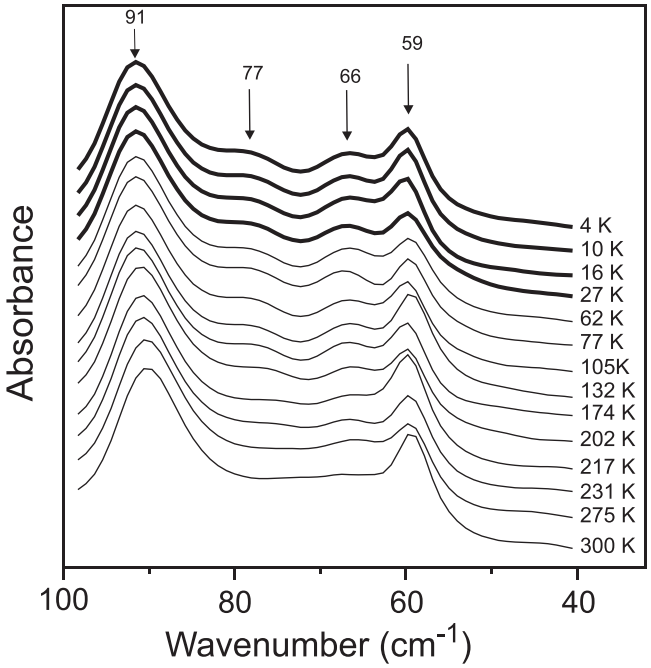

Fig. 5. Temperature transformation of absorption spectra in frequency range 100–40 cm^{-1}. Bold lines correspond to spectra obtained below Neel temperature.

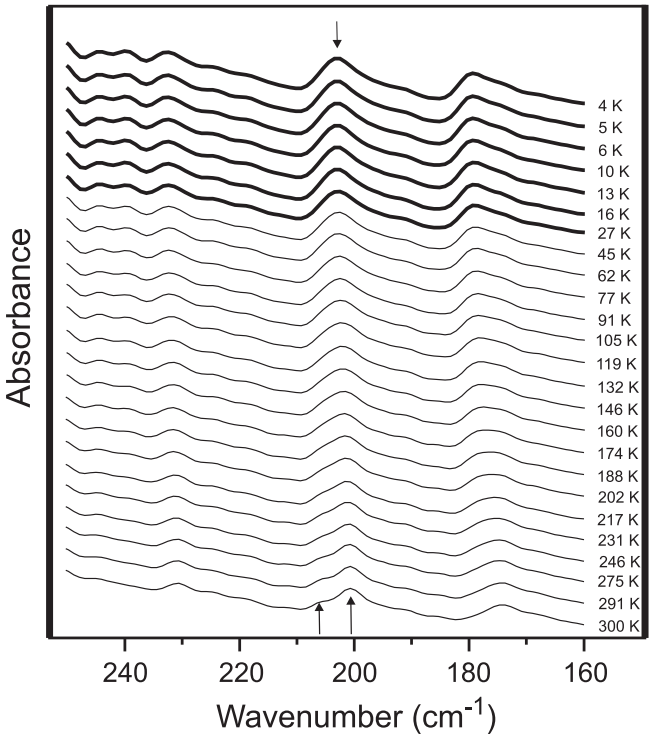

Fig. 6. Temperature transformation of absorption spectra in frequency range 240–160 cm^{-1}. Bold lines correspond to spectra obtained below Neel temperature.

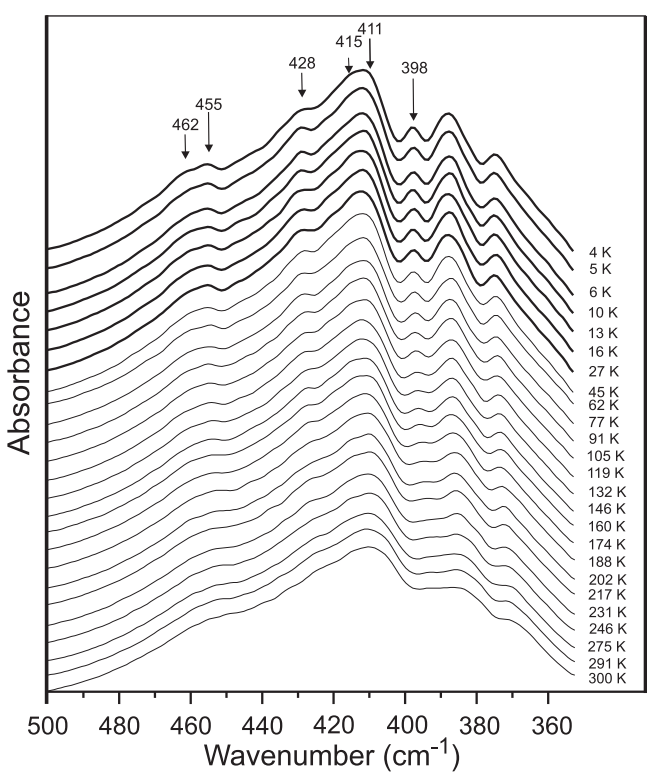

Fig. 7. Temperature transformation of absorption spectra in frequency range 500–360 cm^{-1}. Bold lines correspond to spectra obtained below Neel temperature.

We have not found any other distinct anomalies in IR spectra associated with magnetic ordering of the crystal, as some of them, like magnon effects, are forbidden by crystal symmetry, while others, like shifts of TO modes, seem to be too small to be observed.

5. Conclusion

Our investigations of IR spectra of $HoFe_3(BO_3)_4$ crystal performed over a wide range of frequencies and temperatures showed no Davydov splitting induced by the structural phase transition. This fact is attributed to strong localization of internal vibrations of complexes $(FeO_6)^{9-}$, $(BO_3)^{3-}$ and $(ReO_6)^{9-}$, while most observed vibration modes in the IR spectrum of $HoFe_3(BO_3)_4$ crystal are internal vibrations of these complexes. Higher-frequency IR active vibrational spectrum of $HoFe_3(BO_3)_4$ crystal is formed by ionic complexes $(BO_3)^{3-}$ mainly, deformed by local static crystal field, while their dynamic interactions manifest quite insignificantly.

No effects of magnetic ordering in the IR spectra of the compound under study have been found.

Acknowledgements

The work was partially supported by the RFBR through Grants No. 13-02-00825 and 13-02-98041, SS-4828.2012.2.

References

[1] E.L. Belokoneva, L.I. Alshinskaya, M.A. Simonov, N.I. Leonyuk, T.I. Timchenko, N.V. Belov, Zhurnal Strukturnoi Khimii 20 (1979) 542.
[2] J.A. Campa, C. Cascales, E. Gutierrez-Puebla, M.A. Monge, I. Rasines, C. Ruiz-Valero, Chem. Mater. 9 (1997) 237.
[3] S.A. Klimin, D. Fausti, A. Meetsma, L.N. Bezmaternykh, P.H.M. van Loosdrecht, T.T.M. Palstra, Acta Cryst. B 61 (2005) 481.
[4] A. Brenier, C. Tu, Z. Zhu, B. Wu, Appl. Phys. Lett. 84 (2004) 2034.
[5] X. Chen, Z. Luo, D. Jaque, J.J. Romero, J. Garcia Sole, Y. Huang, A. Jiang, C. Tu, J. Phys.: Condens. Matter 13 (2001) 1171.
[6] A.K. Zvezdin, S.S. Krotov, A.M. Kadomtseva, G.P. Vorb'ev, Y.F. Popov, A.P. Pyatakov, L.N. Bezmaternykh, E.A. Popova, JETP Lett. 81 (2005) 272.
[7] A.K. Zvezdin, G.P. Vorob'ev, A.M. Kadomtseva, Y.F. Popov, A.P. Pyatakov, L.N. Bezmaternykh, A.V. Kuvardin, E.A. Popova, JETP Lett. 83 (2006) 509.
[8] A.M. Kadmotseva, Yu.F. Popov, G.P. Vorobiev, A.P. Pyatakov, S.S. Krotov, K.I. Kamilov, V.Yu. Ivanov, A.A. Mukhin, A.K. Zvezdin, A.M. Kuzmenko, L.N. Bezmaternykh, I.A. Gudim, V.L. Temerov, Low Temp. Phys. 36 (2010) 640–653.
[9] A.K. Zvezdin, S.S. Krotov, A.M. Kadomtseva, G.P. Vorob'ev, Y.F. Popov, A.P. Pyatakov, L.N. Bezmaternykh, E. Popova, JETP Lett. 81 (2005) 272.
[10] M.I. Pashchenko, V.A. Bedarev, V.I. Kutko, L.N. Bezmaternykh, V.L. Temerov, Low Temp. Phys. 36 (2010) 800.
[11] Y. Hinatsu, Y. Doi, K. Ito, K. Wakeshima, A. Alemi, J. Solid State Chem. 172 (2003) 438.
[12] A.S. Krylov, S.N. Sofronova, I.A. Gudim, A.N. Vtyurin, Solid State Commun. 174 (2013) 26.
[13] C. Ritter, A. Vorotynov, A. Pankrats, G. Petrakovskii, V. Temerov, I. Gudim, R. Szymczak, J. Phys.: Condens. Matter 20 (2008) 365209.
[14] D. Fausti, A.A. Nugroho, P.H.M. van Loosdrecht, S.A. Klimin, M.N. Popova, L.N. Bezmaternykh, Phys. Rev. B 74 (2006) 024403.
[15] V.I. Zinenko, M.S. Pavlovskii, A.S. Krylov, I.A. Gudim, E.V. Eremin, J. Exp. Theor. Phys. 117/6 (2013).
[16] R.P. Chaudhury, F. Yen, B. Lorenz, Y.Y. Sun, L.N. Bezmaternykh, V.L. Temerov, C.W. Chu, Phys. Rev. B 80 (2009) 104424.
[17] U. Adem, L. Wang, D. Fausti, W. Schottenhamel, P.H.M. van Loosdrecht, A. Vasiliev, L.N. Bezmaternykh, B. Büchner, C. Hess, R. Klingeler, Phys. Rev. B 82 (2010) 064406.
[18] M.B. Smirnov, V.Yu. Kazimirov, LADY: software for lattice dynamics simulations, JINR Communication E14-2001-159, Dubna, 2001.
[19] K. Nakamoto, Infrared and Raman Spectra of Inorganic and Coordination Compounds. Part A. Theory and Applications in Inorganic Chemistry, John Wiley, New York, 2009, pp. 432.